Journal of Cerebral Blood Flow & Metabolism (2007), 1–14
© 2007 ISCBFM All rights reserved 0271-678X/07 $30.00
www.jcbfm.com

Protective role of reactive astrocytes in brain ischemia

Lizhen Li[1], Andrea Lundkvist[1], Daniel Andersson[1], Ulrika Wilhelmsson[1], Nobuo Nagai[2], Andrea C Pardo[3], Christina Nodin[1], Anders Ståhlberg[4], Karina Aprico[1], Kerstin Larsson[5], Takeshi Yabe[6], Lieve Moons[2], Andrew Fotheringham[7], Ioan Davies[7], Peter Carmeliet[2], Joan P Schwartz[6], Marcela Pekna[5], Mikael Kubista[4], Fredrik Blomstrand[1], Nicholas Maragakis[3], Michael Nilsson[1] and Milos Pekny[1]

[1]*Center for Brain Repair and Rehabilitation, Department of Clinical Neuroscience and Rehabilitation, Institute of Neuroscience and Physiology at Sahlgrenska Academy, Göteborg University, Göteborg, Sweden;* [2]*Flanders Interuniversity Institute for Biotechnology, Center for Transgene Technology & Gene Therapy, KU Leuven, Campus Gasthuisberg, Leuven, Belgium;* [3]*Department of Neurology, Johns Hopkins School of Medicine, Baltimore, Maryland, USA;* [4]*Department of Chemistry and Bioscience, Chalmers University of Technology and TATAA Biocenter, Göteborg, Sweden;* [5]*Department of Medical Chemistry and Cell Biology, Institute of Biomedicine, Sahlgrenska Academy, Göteborg University, Göteborg, Sweden;* [6]*Neurotrophic Factors Section, National Institute of Neurological Disorders and Stroke, National Institutes of Health, Bethesda, Maryland, USA;* [7]*School of Medicine and School of Biological Sciences, University of Manchester, Manchester, UK*

Reactive astrocytes are thought to protect the penumbra during brain ischemia, but direct evidence has been lacking due to the absence of suitable experimental models. Previously, we generated mice deficient in two intermediate filament (IF) proteins, glial fibrillary acidic protein (GFAP) and vimentin, whose upregulation is the hallmark of reactive astrocytes. *GFAP*$^{-/-}$*Vim*$^{-/-}$ mice exhibit attenuated posttraumatic reactive gliosis, improved integration of neural grafts, and posttraumatic regeneration. Seven days after middle cerebral artery (MCA) transection, infarct volume was 210 to 350% higher in *GFAP*$^{-/-}$*Vim*$^{-/-}$ than in wild-type (WT) mice; *GFAP*$^{-/-}$, *Vim*$^{-/-}$ and WT mice had the same infarct volume. Endothelin B receptor (ET_BR) immunoreactivity was strong on cultured astrocytes and reactive astrocytes around infarct in WT mice but undetectable in *GFAP*$^{-/-}$*Vim*$^{-/-}$ astrocytes. In WT astrocytes, ET_BR colocalized extensively with bundles of IFs. *GFAP*$^{-/-}$*Vim*$^{-/-}$ astrocytes showed attenuated endothelin-3-induced blockage of gap junctions. Total and glutamate transporter-1 (GLT-1)-mediated glutamate transport was lower in *GFAP*$^{-/-}$*Vim*$^{-/-}$ than in WT mice. DNA array analysis and quantitative real-time PCR showed down-regulation of plasminogen activator inhibitor-1 (PAI-1), an inhibitor of tissue plasminogen activator. Thus, reactive astrocytes have a protective role in brain ischemia, and the absence of astrocyte IFs is linked to changes in glutamate transport, ET_BR-mediated control of gap junctions, and PAI-1 expression.
Journal of Cerebral Blood Flow & Metabolism advance online publication, 29 August 2007; doi:10.1038/sj.jcbfm.9600546

Keywords: astrocytes; GFAP; intermediate filaments; reactive gliosis (astrogliosis); vimentin

Correspondence: Dr M Pekny, Department of Clinical Neuroscience and Rehabilitation, Institute of Neuroscience and Physiology, Sahlgrenska Academy at Göteborg University, Göteborg SE-405 30, Sweden. E-mail: Milos.Pekny@neuro.gu.se
This study was supported by grants from the Swedish Research Council (11548 to Mpy, 5174 to UW, 13470 to MPa and 20114 to MN), The Region of Västra Götaland (RUN), the Swedish Cancer Foundation (3622), ALF Göteborg, Hjärnfonden, the Swedish Stroke Association, Torsten and Ragnar Söderberg's Foundations, Frimurare Foundation, Rune and Ulla Amlöv's Foundation, Trygghansa, the Swedish Society for Medicine, the Swedish Society for Medical Research, the King Gustaf V Foundation, Volvo Assar Gabrielsson Fond, and the Novo Nordisk Foundation Program on Diabetic Microangiopathy, STINT Sweden, Edit Jacobsson's Foundation, Axel Linder's Foundation, and Carl Trigger's Foundation.
Received 11 May 2007; revised 27 June 2007; accepted 16 July 2007

Introduction

Astroglial cells are the most abundant cells in the central nervous system (CNS) and are believed to play a major role in the brain and spinal cord pathologies. Although never proved directly, astrocytes are thought to exert a neuroprotective effect in stroke by shielding neurons from oxidative stress (Kraig *et al*, 1995). This hypothesis is based on the ability of astrocytes to engage in spatial buffering, to transport and metabolize amino acids, glucose, and other key molecules, and to upregulate antioxidants and free radical scavengers in the ischemic region.

Reactive gliosis is a response of astrocytes to CNS injury, including brain ischemia, mechanical

trauma, neurodegenerative diseases, and tumors. Reactive astrocytes undergo changes in morphology and in their expression of a wide range of molecules (Eddleston and Mucke, 1993; Ridet *et al*, 1997). The hallmark of reactive gliosis, regardless of its origin, is increased expression of glial fibrillary acidic protein (GFAP) and vimentin in reactive astrocytes. Glial fibrillary acidic protein and vimentin are building blocks of intermediate filaments (IFs), which, together with microtubules and actin filaments, constitute the cytoskeleton.

We and others have generated *GFAP*$^{-/-}$ mice (Gomi *et al*, 1995; Liedtke *et al*, 1996; McCall *et al*, 1996; Pekny *et al*, 1995) and found that their astrocytes are free of IFs in the absence of any challenge, since vimentin requires GFAP to polymerize into filaments (Pekny *et al*, 1995). However, reactive astrocytes in *GFAP*$^{-/-}$ mice contain IFs because they also produce nestin, an IF protein that copolymerizes with vimentin in both *GFAP*$^{-/-}$ and wild-type (WT) reactive astrocytes (Eliasson *et al*, 1999; Pekny *et al*, 1998*a*). *GFAP*$^{-/-}$ mice exhibit normal healing after brain and spinal cord injury (Pekny *et al*, 1999*b*; Pekny *et al*, 1995). In mice lacking both GFAP and vimentin (*GFAP*$^{-/-}$*Vim*$^{-/-}$), however, reactive astrocytes are devoid of IFs, reflecting the inability of nestin to self-polymerize (Eliasson *et al*, 1999). As a result, reactive gliosis and glial scar formation after neurotrauma in the brain or spinal cord are attenuated (Pekny *et al*, 1999*b*; Pekny and Pekna, 2004). After neurotrauma, IF-free astrocytes of *GFAP*$^{-/-}$*Vim*$^{-/-}$ mice reach comparable volume of tissue as WT astrocytes; however, *GFAP*$^{-/-}$*Vim*$^{-/-}$ astrocytes show less prominent thickening of the main cellular processes (Wilhelmsson *et al*, 2004). Posttraumatic regeneration of neuronal synapses (Wilhelmsson *et al*, 2004) and integration of neural grafts (Kinouchi *et al*, 2003) were improved in *GFAP*$^{-/-}$*Vim*$^{-/-}$ mice, despite more prominent synaptic loss at the initial stage after neurotrauma (Wilhelmsson *et al*, 2004).

In this study, we subjected *GFAP*$^{-/-}$*Vim*$^{-/-}$, *GFAP*$^{-/-}$, and *Vim*$^{-/-}$ mice to brain ischemia induced by middle cerebral artery (MCA) transection by two independent paradigms. After 7 days of ischemia, infarct volumes were 2- to 3.5-fold larger in *GFAP*$^{-/-}$*Vim*$^{-/-}$ mice than in WT, *GFAP*$^{-/-}$, or *Vim*$^{-/-}$ mice. This increase correlated with reduced glutamate uptake in cortical slices from *GFAP*$^{-/-}$*Vim*$^{-/-}$ mice, altered endothelin B receptor (ET_BR)-mediated control of gap junctions, and downregulation of plasminogen activator inhibitor-1 (PAI-1) in *GFAP*$^{-/-}$*Vim*$^{-/-}$ cultures. These findings suggest that reactive astrocytes have a protective role in brain ischemia.

Materials and methods

Mice

Single-mutant (*GFAP*$^{-/-}$ or *Vim*$^{-/-}$), double-mutant (*GFAP*$^{-/-}$*Vim*$^{-/-}$), and WT control mice were maintained on a mixed C57Bl/129 genetic background as described (Eliasson *et al*, 1999; Pekny *et al*, 1999*b*). All mice were age-matched adults except for the preparation of astrocyte-enriched cultures for which postnatal day 1 to 2 mice were used. The mice were kept in a barrier animal facility and fed *ad libitum*.

Induction of Ischemia: Proximal Middle Cerebral Artery Transection

Focal cerebral ischemia was induced in six WT and six *GFAP*$^{-/-}$*Vim*$^{-/-}$ mice by proximal MCA transection as described (Fotheringham *et al*, 2000) with slight modifications. Mice were anesthetized with isoflurane in oxygen, and body temperature was maintained at 37°C with a heating pad. Under the operating microscope, the left MCA was exposed, occluded at two points by bipolar coagulation, and transected to ensure permanent disruption (Figure 1E). The proximal end of the MCA (A) was coagulated approximately 2.5 mm from the MCA/anterior cerebral artery branch (as determined after brain dissection). After surgery, mice were housed individually in cages that were placed on a heating pad. After 1 h, the mice were returned to their normal environment.

Induction of Ischemia: Distal Middle Cerebral Artery Transection

Distal MCA transection was performed as described (Nagai *et al*, 1999) in two independent series of experiments. One set of experiments was performed in 10 WT and 11 *GFAP*$^{-/-}$*Vim*$^{-/-}$ mice. To determine if partial deficiency of astrocyte IFs or a deficiency of IFs in endothelial cells also affected the infarct volume, a second set of experiments was performed in nine WT, nine *GFAP*$^{-/-}$, eight *Vim*$^{-/-}$, and nine *GFAP*$^{-/-}$*Vim*$^{-/-}$ mice. Briefly, mice were anesthetized by intraperitoneal injection of ketamine (75 mg/mL; Apharmo, Arnhem, The Netherlands) and xylazine (5 mg/mL; Bayer, Leverkusen, Germany), and body temperature was maintained at 37°C with a heating pad. Under the operating microscope, the MCA was ligated with a 10-0 suture Ethylon nylon thread (Ethylon, Neuilly, France) and transected distally (Figure 1E). After surgery, the mice were returned to their cages, which were placed on a heating pad (37°C) for 1 h.

Measurement of Infarct Volume 7 Days after Proximal Middle Cerebral Artery Transection

Deeply anesthetized mice were killed by decapitation. Fresh frontal brain slices (0.5 mm thick) were cut on a Vibratome, incubated for 30 mins in 0.125% triphenyltetrazolium chloride solution (T4375; Sigma-Aldrich, St Louis, MO, USA) in buffer containing 1.35% dimethylsulfoxide, 2 mmol/L $MgCl_2$, 0.1 mol/L Na_2HPO_4, and 0.1 mol/L NaH_2PO_4 (pH 7.4) at 37°C, and fixed in 4% buffered formaldehyde (pH 7.4) (Fotheringham *et al*, 2000). In each slice, the infarct area in white matter was measured with a Nikon SMZ-U stereomicroscope and

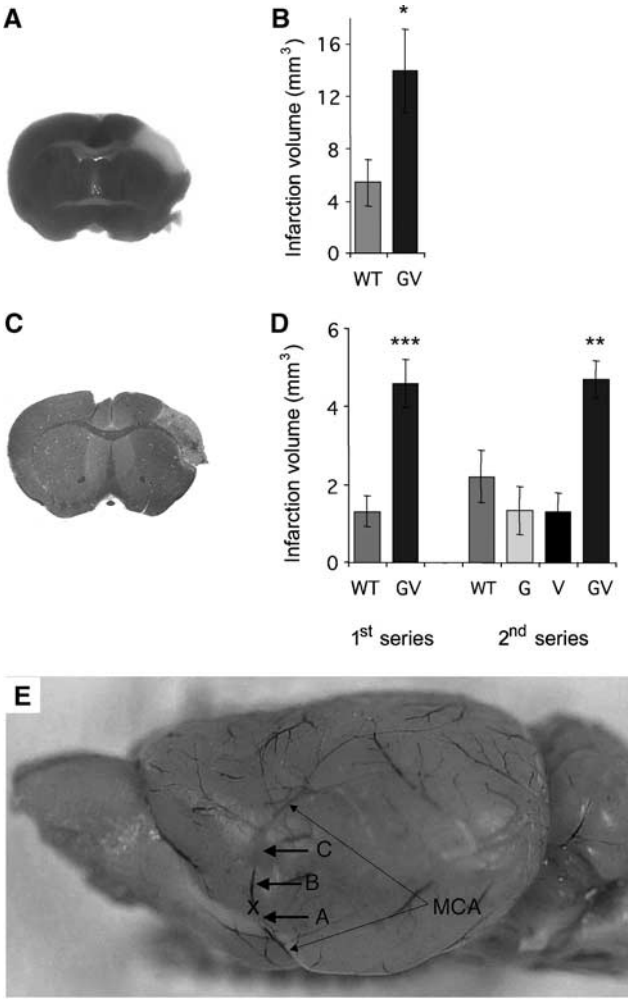

Figure 1 Infarct area is 2.5- to 3.5-fold larger in *GFAP*$^{-/-}$*Vim*$^{-/-}$ (GV) than in WT mice 7 days after MCA transection. The infarct area was visualized by triphenyltetrazolium chloride and hematoxylin/erythrosin staining 7 days after proximal (**A**) and distal (**C**) transection of the MCA. (**B** and **D**) Infarct volume was more than two-fold larger in *GFAP*$^{-/-}$*Vim*$^{-/-}$ than in WT mice (**B**, $*P < 0.05$; **D**, $***P < 0.001$ and $**P < 0.01$). (**D**) In *GFAP*$^{-/-}$ (G) and *Vim*$^{-/-}$ (V) mice, the infarct volume was not significantly different from that in WT mice. (**E**) Proximal MCA transection was performed at point X after bipolar coagulation at points A and B. Distal MCA transection was performed at point C (approximately 1.5 mm distal to point A). Values are mean ± s.e.m.

image analysis software (Easy Image, Bergström Instrument, Göteborg, Sweden). The infarct volume was calculated by integrating infarct areas on all adjacent brain slices with detectable infarction. The extent of brain edema was judged by comparing the areas of the ischemic and contralateral hemispheres.

Measurement of Infarct Volume 7 Days after Distal Middle Cerebral Artery Transection

Deeply anesthetized mice were perfused through the left ventricle with 4% phosphate-buffered formaldehyde (pH 7.4). The brains were postfixed overnight and embedded in paraffin. Frontal sections (8 μm thick) were stained with hematoxylin and erythrosine. Infarct areas were assessed by delineating the ischemic region, which could be clearly discriminated by its lighter appearance and high proportion of cells with pycnotic nuclei. The infarct area was measured on all sections (320 μm apart) on which it was detectable (4 to 10 sections per mouse) as described above, and the total infarct volume was calculated.

Blood Pressure and Heart Rate Monitoring

Blood pressure and heart rate were monitored in five WT and four *GFAP*$^{-/-}$*Vim*$^{-/-}$ mice during the distal MCA transection. Under isoflurane anesthesia, the 10-0 suture Ethylon nylon thread (Ethylon, France) was passed under the MCA. The mouse was turned on its back, an incision was made in the neck, the left common carotid artery was exposed, and a 2.5F catheter was inserted and connected to a clinical fluid-filled discardable transducer (HLT0698; Fysicon, Oss, The Netherlands). Signal from the transducer was collected with an AD converter (PowerLab, ADInstruments, Chalgrove, UK). After measurement of baseline blood pressure and heart rate, the MCA was occluded by tightening the suture around the vessel. Blood pressure and heart rate were recorded 10 s, 15 mins, 30 mins, and 1 h after the MCA occlusion. After the operation, the mice were kept on a heating pad (37°C) for 1 h and were given free access to water and food. After 7 days, the mice were anesthetized with ketamine (75 mg/mL; Apharmo) and xylazine (5 mg/mL; Bayer) and perfused first with phosphate-buffered saline (PBS) for 7 mins and then with 4% phosphate-buffered formaldehyde (pH 7.4). The brains were postfixed overnight and embedded in paraffin.

Comparison of Cerebrovascular Architecture

The MCA territory was determined as described (Maeda *et al*, 1998). Briefly, the cerebrovasculature of four WT and four *GFAP*$^{-/-}$*Vim*$^{-/-}$ mice, 8-month-old, was visualized by detection of endothelial cells with a rat anti-CD-31 antibody (1:200; BD Biosciences, San Jose, CA, USA) and a horseradish peroxidase-conjugated secondary antibody (P0162, 1:100; Dako, Glostrup, Denmark) according to standard immunohistochemical procedures; endogenous peroxidase activity was blocked by incubating the brains with PBS containing 0.6% H_2O_2 for 30 mins, and antibody incubations were performed at 4°C overnight. The distance between the dorsal midline and the line of anastomoses connecting the peripheral branches of the MCA and the anterior cerebral artery was measured at three points (2, 4, and 6 mm from the frontal pole) with the Nikon SMZ-U stereomicroscope and image analysis software (Easy Image).

Data Analysis

Data are expressed as mean ± s.e.m. The two-tailed *t*-test was used for statistical analysis. Differences were considered significant at $P < 0.05$.

Immunohistochemistry

Coronal cryosections (35 μm), made from perfused and postfixed brains of four WT and three *GFAP*$^{-/-}$*Vim*$^{-/-}$ mice, were incubated in 0.05% glycine in PBS for 1 h at room temperature and permeabilized overnight in PBS containing 0.5% Tween 20 and 1% bovine serum albumin at room temperature. S100β and ET_BR were detected with rabbit antibodies against S100β (Z0311, 1:200; Dako) and ET_BR (1:100; Alomone Labs, Jerusalem, Israel) and Alexa 488-conjugated anti-rabbit antibodies (1:500; Molecular Probes, Eugene, OR, USA). Glial fibrillary acidic protein and glutamine synthase (GS) were detected with mouse antibodies against GFAP (clone GA5, 1:100; Sigma-Aldrich) and GS (1:100; Chemicon Europe Ltd, Hampshire, UK), and Alexa 568-conjugated anti-mouse antibodies (1:500; Molecular Probes). Glutamate transporter-1 (GLT-1) was detected with guinea-pig antibodies against GLT-1 (1:100; Chemicon Europe Ltd.) and Alexa 488-conjugated anti-guinea pig antibodies (1:100; Molecular Probes). Microglia were detected with biotinylated tomato lectin (30 μg/mL; Sigma-Aldrich) and Cy3-conjugated streptavidin (1:100; Sigma-Aldrich). Antibodies were diluted in 1% bovine serum albumin and 0.01% Tween 20 in PBS. Cell nuclei were stained with ToPro-3 (1:1,000; Molecular Probes).

Astrocyte-Enriched Cultures

Primary astrocyte-enriched cultures were prepared from postnatal day 1 *GFAP*$^{-/-}$*Vim*$^{-/-}$ and WT mice as described (Pekny *et al*, 1998*a*). The cultures for immunocytochemistry were grown in 16-chamber slides (Nalge Nunc International, Naperville, IL, USA) in Dulbecco's modified Eagle's medium (D5671; Sigma-Aldrich) containing 10% fetal calf serum, 2 mmol/L L-glutamine, and penicillin–streptomycin (Invitrogen, Paisley, UK). Cultures for quantitative real-time PCR analysis of mRNA were maintained in 10% fetal calf serum (ET_BR and connexin 43 (Cx43)) or 1 or 10% fetal calf serum (PAI-1).

Immunocytochemistry

Cells were fixed in methanol at -20°C for 5 mins and washed with PBS. After nonspecific binding was blocked with 5% normal goat serum (Dako) for 15 mins at room temperature, cells were incubated with rabbit antibodies against ET_BRs (1:100; Alomone Labs) and mouse antibodies against GFAP (clone GA5, 1:100; Sigma-Aldrich) and then with Alexa 488-conjugated anti-rabbit and Alexa 568-conjugated anti-mouse antibodies (1:500; Molecular Probes). All antibodies were diluted in PBS.

Sodium Dodecyl Sulfate-Polyacrylamide Gel Electrophoresis and Immunoblotting for Endothelin B Receptors

Medium was removed from confluent cultures of astrocytes (10 to 14 days after plating). After two washes with PBS, cells were harvested by scraping into sodium dodecyl sulfate-extraction buffer consisting of protease inhibitor cocktail (Roche, Mannheim, Germany), 1 mmol/L Na^+ orthovanadate, and 1 mmol/L phenylmethanesulfonyl in 2% sodium dodecyl sulfate, and the cell lysate was frozen at -80°C. Thawed lysates were sonicated for 5 secs, and the protein content was determined with the Bicinchoninic Acid Protein Assay (Sigma-Aldrich). Protein (50 μg) was separated on 4 to 12% bis-Tris gels (Invitrogen, Carlsbad, CA, USA) and transferred to a nitrocellulose membrane. The membrane was stained with Ponceau S solution (Sigma-Aldrich) to control for equal protein loading. ET_BRs were detected with polyclonal rabbit antibodies (1:500; Alomone Labs), and β-actin (internal loading control) was detected with a mouse monoclonal antibody (1:1,000; Abcam, Cambridge, UK). To enhance the signal for ET_BR, the immunoblot was incubated with biotin-conjugated monoclonal anti-rabbit immunoglobulins (Sigma-Aldrich) and probed with peroxidase-conjugated streptavidin (Dako) or with peroxidase-conjugated donkey anti-mouse immunoglobulins for β-actin detection (Jackson Immunoresearch, Suffolk, UK). Immunoreactivity was visualized by chemiluminescence and quantified with Multi Gauge v2.3 software (Fuji Photo Film Co., Ltd, Tokyo, Japan). Band densities were compared by one-way analysis of variance followed by Bonferroni's multiple comparison test performed with the SPSS statistical package v11.5.1 (SPSS, Chicago, IL, USA).

Reverse Transcription and Quantitative Real-Time PCR

cDNA was generated using the iScript cDNA Synthesis Kit (Bio-Rad Laboratories, Hercules, CA, USA) with a mixture of random hexamers and oligo(dT) primers, according to the manufacturer's instructions, except that for ET_BR and Cx43 expression analyses, the incubation time at 42°C was increased from 30 to 60 mins. The reverse transcription was run in duplicate in 10-μL reactions (Stahlberg *et al*, 2004) using 1.5 μg of total RNA extracted from primary astrocyte cultures as described below. The cultures were prepared from four WT and four *GFAP*$^{-/-}$*Vim*$^{-/-}$ mice (for ET_BR and Cx43), and five WT and three *GFAP*$^{-/-}$*Vim*$^{-/-}$ mice (for PAI-1). Gene-specific SYBR-Green I-based PCR assays were designed for ET_BR (GenBank accession number NM_007904), PAI-1 (GenBank accession number M33960), and Cx43 (GenBank accession number M63801). Formation of expected PCR products was confirmed with agarose gel electrophoresis and melting curve analysis. The primer sequences were as follows: 5′-AAGAATGCC CAAGAGAAAAC-3′ (forward) and 5′-AAAAAGGAAGGA AGGAAAATC-3′ (reverse) for ET_BR; 5′-CAGACAATG GAA GGGCAACA-3′ (forward) and 5′-GCGGGCTGAGATGAC AAA-3′ (reverse) for PAI-1; and 5′-ACCCAACAGCAGCA GACTT-3′ (forward) and 5′-ACCGACAGCCACACCTTC-3′ (reverse) for Cx43. Real-time PCR experiments were run on a Rotor-Gene 3000 (Corbett Research, Sydney, Australia) and were analyzed as described (Stahlberg *et al*, 2004). All gene expression data were normalized to total RNA concentration. The statistical significance of differences between *GFAP*$^{-/-}$*Vim*$^{-/-}$ and WT mice was tested

with two-tailed *t*-tests. Polymerase chain reaction run conditions and thermocycler programs are available on request.

Scrape Loading/Dye Transfer

Astrocyte gap-junctional communication (AGJC) was assessed by using the scrape loading/dye transfer technique as described (Blomstrand *et al*, 1999). In brief, confluent astrocyte cultures from five WT and four *GFAP*$^{-/-}$*Vim*$^{-/-}$ mice were incubated for 7 mins in HEPES (4-(2-hydroxyethyl)-1-piperazineethanesulfonic acid)-buffered salt solution (137 mmol/L NaCl, 5.4 mmol/L KCl, 0.41 mmol/L $MgSO_4$, 0.49 mmol/L $MgCl_2$, 1.26 mmol/L $CaCl_2$, 0.64 mmol/L KH_2PO_4, 3 mmol/L $NaHCO_3$, 5.5 mmol/L glucose, and 20 mmol/L HEPES (pH 7.4)), with or without a nonsaturating dose of 10 nmol/L of endothelin-3 in this and subsequent steps, and followed by four quick washes in Ca^{2+}-free buffer. Lucifer yellow (0.1% w/v) in Ca^{2+}-free buffer was added, and two parallel scrapes were performed with a scalpel. The Lucifer yellow was removed after 1 min, and Ca^{2+}-containing buffer was added. 8 mins after scraping, four images from each culture were captured with a Nikon Optiphot 2 equipped with a Hamamatsu C5810 chilled three-chip color charge-coupled device camera. The dye spread was quantitated by using Easy Image Analysis 2000 (Tekno Optik AB, Stockholm, Sweden) to measure the fraction of a predefined area occupied by Lucifer yellow-positive cells.

Glutamate Uptake

Fresh brain slices microdissected from five WT and nine *GFAP*$^{-/-}$*Vim*$^{-/-}$ mice were homogenized in 5 mmol/L Tris/320 mmol/L sucrose with a protease inhibitor cocktail (Complete; Roche, Indianapolis, IN, USA), using a hand-held pellet pistol. Samples were then washed three times in ice-cold PBS (pH 7.4) and resuspended in Na^+-containing Krebs buffer (120 mmol/L NaCl, 25 mmol/L Tris–HCl, pH 7.4, 5 mmol/L KCl, 2 mmol/L $CaCl_2$, 1 mmol/L KH_2PO_4, 1 mmol/L $MgSO_4$, and 10% glucose) or in Na^+-free Krebs (120 mmol/L choline-Cl substituted for NaCl). The samples were then incubated with 10 μmol/L ^{3}H-glutamate for 4 mins at 37°C, harvested with a tissue harvester (Brandel, Gaithersburg, MD, USA) on a Whatman GF/B paper (FPD-100; Brandel), and washed three times in Tris buffer (pH 7.4). Radioactivity was determined by standard scintillation counting. Mean Na^+-dependent uptake was determined in duplicate by subtracting the mean uptake in a Na^+-free duplicate. To determine the contribution of GLT-1-mediated transport, a separate set of samples was also incubated with 500 μmol/L dihydrokainate and 10 μmol/L ^{3}H-glutamate for 4 mins at 37°C, harvested, and washed three times in Tris buffer (pH 7.4) on the Whatman GF/B paper using a tissue harvester. Radioactivity and mean Na^+-dependent uptake were determined as described above.

Sodium Dodecyl Sulfate-Polyacrylamide Gel Electrophoresis and Immunoblotting for Glutamate Transporter-1

Brain slices (approximately 2×2 mm) taken from the cortex of the left hemisphere of six WT and nine *GFAP*$^{-/-}$*Vim*$^{-/-}$ mice were homogenized by sonication in Tris-EDTA (ethylenediaminetetraacetic acid) buffer containing protease inhibitors (aprotinin, pepstatin, and leupeptin). Samples were stored at −70°C until use. Aliquots of homogenized samples (1 to 20 μg protein) were subjected to sodium dodecyl sulfate-polyacrylamide gel electrophoresis (8% polyacrylamide gels) and transferred to nitrocellulose membranes (Hybond ECL, Amersham, Buckinghamshire, UK) by electroblotting (100 V, 60 mins). Western blot analysis was performed as described (Rothstein *et al*, 1994). In brief, blots were blocked and washed in 50 mmol/L Tris-buffered saline containing 5% nonfat milk and 0.5% Tween 20, and probed with affinity-purified polyclonal antibodies specific for GLT-1 (1:10,000; C terminus-directed antibody) using horseradish peroxidase-conjugated donkey anti-rabbit IgG (1:5,000; Amersham) as secondary antibody. The blots were also probed for actin (1:2,000) as a protein-loading standard. In all cases, protein levels varied by <10% between lanes. Immunoreactivity was visualized by enhanced chemiluminescence and quantified densitometrically with Quantity One v4.0 software (Bio-Rad Laboratories).

DNA Array Analysis

RNA extraction, DNase treatment, poly (A+) RNA enrichment, probe synthesis, column chromatography, and hybridization of the probes to the array were performed as described in the Atlas Pure Total RNA Labeling System User Manual and the Atlas cDNA Expression Arrays User Manual (Clontech Laboratories, Palo Alto, CA, USA). Confluent astrocyte cultures were harvested by scraping into RNase-free PBS and centrifuged at 500*g* for 5 mins at 4°C. The arrays were exposed to phosphor screens (Molecular Dynamics, Buckinghamshire, UK) overnight. The screens were scanned in a Storm instrument (Storm 820, Molecular Dynamics), and the images were analyzed with AtlasImage 1.5 (Clontech Laboratories).

Results

Larger Infarct Volume in *GFAP*$^{-/-}$*Vim*$^{-/-}$ than WT Mice after Proximal Middle Cerebral Artery Transection

Seven days after proximal MCA transection, infarct volume was 257% higher in *GFAP*$^{-/-}$*Vim*$^{-/-}$ mice than in WT controls (14.0 ± 3.20 vs 5.43 ± 1.81 mm^3, $P < 0.05$; Figures 1A and 1B). No difference was found in the extent of brain edema (1.00 ± 0.08 vs 1.04 ± 0.08, respectively).

Larger Infarct Volume in *GFAP*$^{-/-}$*Vim*$^{-/-}$ than WT Mice after Distal Middle Cerebral Artery Transection

To determine if the transection point affects the difference in the infarct volume between WT and *GFAP*$^{-/-}$*Vim*$^{-/-}$ mice, we transected the MCA more distally (Figure 1E). In the first set of experiments, the infarct volume was 351% larger in *GFAP*$^{-/-}$*Vim*$^{-/-}$ than in WT mice 7 days after distal MCA transection (4.60 ± 0.62 vs $1.31 \pm 0.40\,mm^3$, $P < 0.001$; Figures 1C and 1D). To determine if partial deficiency of IFs in astrocytes or deficiency of IFs in endothelial cells also affected the infarct volume, single *GFAP*$^{-/-}$ and *Vim*$^{-/-}$ mice were included in a second experimental series. The infarct volume was 214% larger in *GFAP*$^{-/-}$*Vim*$^{-/-}$ than in WT mice (4.71 ± 0.62 vs $2.20 \pm 0.40\,mm^3$, $P < 0.01$; Figure 1D), and there were no significant differences in the infarct volume between *GFAP*$^{-/-}$ and *Vim*$^{-/-}$ mice (1.34 ± 0.62 and $1.32 \pm 0.46\,mm^3$, respectively) and WT mice (Figure 1D).

Median Blood Pressure and Heart Rate and Cerebrovascular Architecture are not Altered in *GFAP*$^{-/-}$*Vim*$^{-/-}$ Mice

To address a possible primary effect of the absence of GFAP and Vim on blood pressure and cerebrovascular architecture, we recorded blood pressure and heart rate during and after the MCA transection and compared the anastomoses between branches of the MCA and the anterior cerebral artery. During the MCA transection and for 60 mins thereafter, mean blood pressure and heart rate did not differ in WT and *GFAP*$^{-/-}$*Vim*$^{-/-}$ mice (data not shown). The lines of anastomoses between branches of the MCA and the anterior cerebral artery were comparable in WT and *GFAP*$^{-/-}$*Vim*$^{-/-}$ mice (Figure 2).

Normal Number of Astrocytes and Microglia in the Penumbra of *GFAP*$^{-/-}$*Vim*$^{-/-}$ Mice

Next, we examined the penumbra and the infarct area histologically. Except for the larger infarct area in *GFAP*$^{-/-}$*Vim*$^{-/-}$ mice, hematoxylin/erythrosine staining showed no difference in the appearance of the penumbra and the infarct region between WT and *GFAP*$^{-/-}$*Vim*$^{-/-}$ mice. Immunostaining for S100β revealed comparable numbers of astrocytes in the two groups (62.13 ± 3.29 vs 57.33 ± 3.44 per $0.25\,mm^2$ for WT and *GFAP*$^{-/-}$*Vim*$^{-/-}$ mice, respectively; $P = 0.37$), although *GFAP*$^{-/-}$*Vim*$^{-/-}$ astrocytes had less prominent hypertrophy of the main cellular processes (Figures 3A and 3B). Comparable numbers of astrocytes in the two groups were also confirmed by GS immunostaining (data not shown). Tomato lectin staining showed no differences in the appearance, distribution, and number of microglial cells in the penumbra and the infarct region between WT and *GFAP*$^{-/-}$*Vim*$^{-/-}$ mice (54.5 ± 2.84 vs 61.33 ± 5.24 per $0.0625\,mm^2$, respectively; $P = 0.27$ and data not shown).

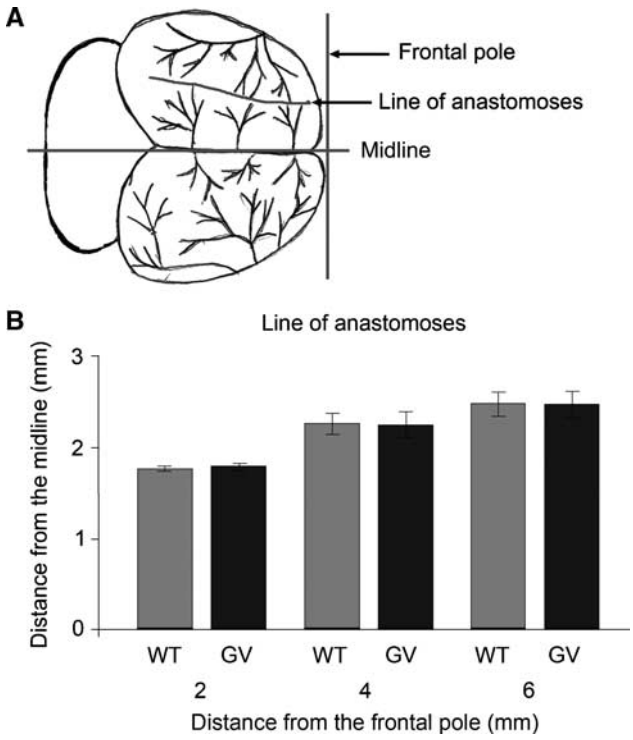

Figure 2 The territory supplied by the MCA is comparable in WT and *GFAP*$^{-/-}$*Vim*$^{-/-}$ (GV) mice. Comparison of the line of anastomoses (**A**) at 2, 4, and 6 mm from the frontal pole (**B**). Values are mean $\pm$ s.e.m.

Absence of Endothelin B Receptor-Immunoreactivity in Astrocytes in the Ischemic Penumbra of *GFAP*$^{-/-}$*Vim*$^{-/-}$ Mice

Endothelin B receptor expression by astrocytes in the injured CNS was proposed as one of the steps leading to astrocyte activation and reactive gliosis (Koyama *et al*, 1999). In the ischemic penumbra and in the corpus callosum 7 days after MCA transection, ET_BRs were highly expressed on reactive astrocytes in WT mice (Figures 3E and 3K) but were essentially undetectable on astrocytes of *GFAP*$^{-/-}$*Vim*$^{-/-}$ mice (Figures 3F and 3L). Similarly, in WT astrocytes in cultures prepared from postnatal day 1 mouse brains, ET_BRs were readily detectable and the ET_BR immunoreactivity exhibited a characteristic filamentous appearance (Figure 4). In contrast, ET_BR immunoreactivity was undetectable in the cytoplasm of *GFAP*$^{-/-}$*Vim*$^{-/-}$ astrocytes (Figure 4). Interestingly, numerous *GFAP*$^{-/-}$*Vim*$^{-/-}$ astrocytes exhibited a granular ET_BR immunoreactivity in the cell nucleus (Figure 4). This finding suggests that IFs are required for the

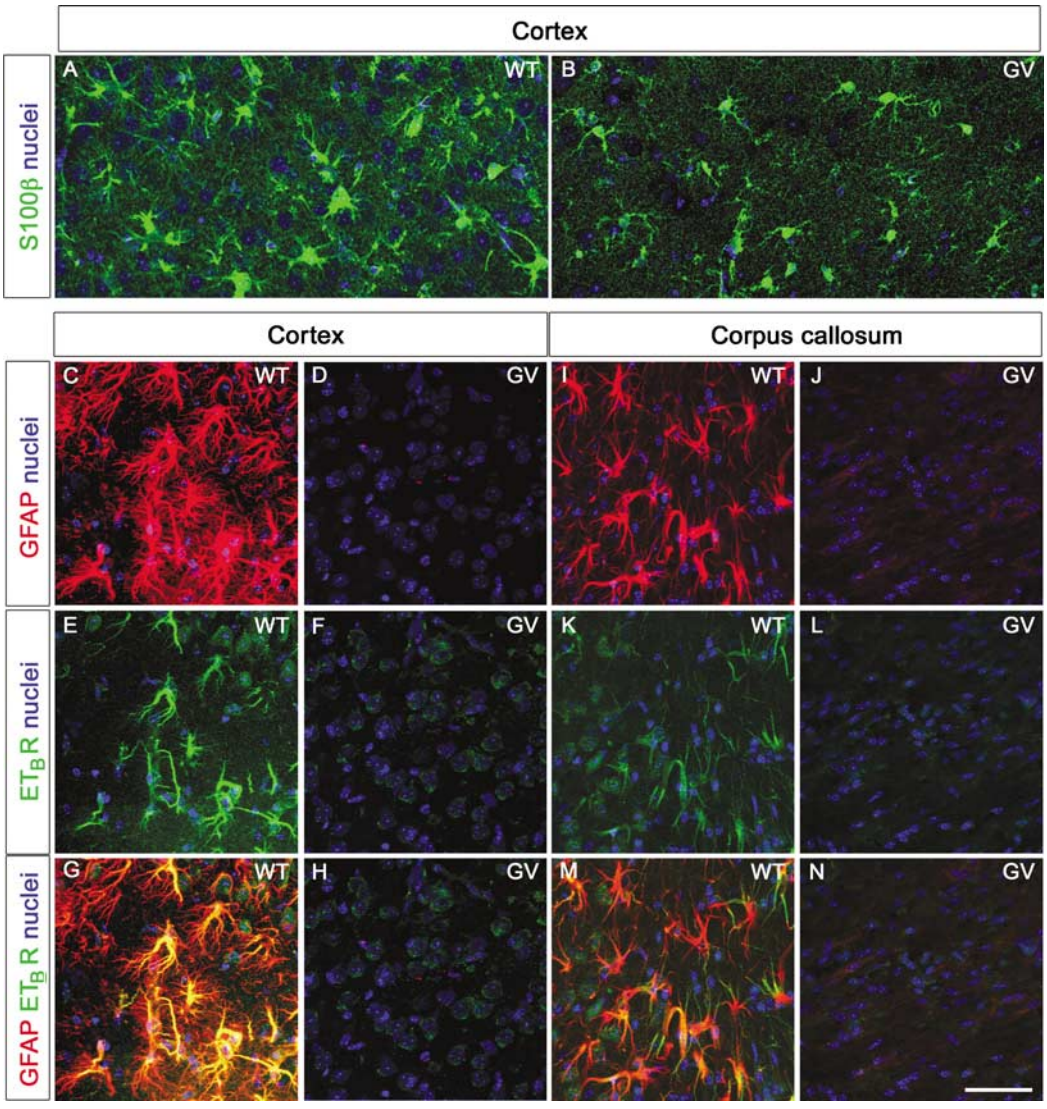

Figure 3 Astrocytes around the ischemic lesion show ET_BR immunoreactivity in WT but not *GFAP*$^{-/-}$*Vim*$^{-/-}$ (GV) mice. (**A** and **B**) No difference was detected in the distribution of astrocytes in the penumbra in the two groups, although astrocytes of *GFAP*$^{-/-}$*Vim*$^{-/-}$ mice showed less prominent hypertrophy of cellular processes. Green, S100β; blue, cell nuclei visualized by ToPro-3. Reactive astrocytes adjacent to the ischemic lesion in WT mice (visualized by antibodies against GFAP, **C** and **I**) were ET_BR-positive (**E** and **K**) 7 days after MCA transection. (**F** and **L**) In contrast, no ET_BR immunoreactivity was detected in astrocytes in *GFAP*$^{-/-}$*Vim*$^{-/-}$ mice. (**G** and **M**) Merged images of (**C** and **E**) and of (**I** and **K**), respectively. (**C** to **N**) Red, GFAP; green, ET_BR; blue, nuclei visualized by ToPro-3. Scale bar = 50 μm.

production, stability, or distribution of ET_BRs in reactive astrocytes.

Endothelin B Receptor Immunoreactivity Colocalizes with Intermediate Filament Bundles in Reactive Astrocytes

To investigate further the relationship between ET_BR and astrocyte IFs, we analyzed their distributions in cultured astrocytes by laser-scanning confocal microscopy. This analysis revealed remarkable colocalization between bundles of IFs and ET_BR immunoreactivity in WT astrocytes, with the ET_BR immunoreactivity decorating bundles of IFs (Figure 5).

Intermediate Filaments Determine Endothelin B Receptor Distribution in Reactive Astrocytes

To determine if IFs are required for the production, stability, or distribution of ET_BR in reactive astrocytes, we performed quantitative real-time PCR and Western blot analyses on cultured astrocytes from *GFAP*$^{-/-}$*Vim*$^{-/-}$ and WT mice. Endothelin B receptor mRNA levels were 43% higher in *GFAP*$^{-/-}$*Vim*$^{-/-}$ than in WT astrocytes ($P<0.05$), but the amounts of ET_BR protein were comparable (Figure 6). Thus, in the absence of IFs, astrocytes contain a normal amount of ET_BRs, which do not associate with IFs but seem to be distributed throughout the cell.

Endothelin-3-Induced Blockage of Gap Junctions is Attenuated in *GFAP*$^{-/-}$*Vim*$^{-/-}$ Astrocytes

Endothelins are well-known blockers of astrocyte gap-junctional communication (AGJC) (Blomstrand *et al*, 1999). To determine if the altered cytoplasmic distribution of ET_BRs affects AGJC and thus the function of the astrocyte syncytium, we stimulated ET_BRs with the selective ligand endothelin-3. No significant difference in basal AGJC was observed between WT and *GFAP*$^{-/-}$*Vim*$^{-/-}$ astrocytes, but endothelin-3-mediated inhibition of AGJC was less prominent in *GFAP*$^{-/-}$*Vim*$^{-/-}$ than in WT astrocytes (72.3 ± 8.9 vs 39.8 ± 2.6% of control levels; $P < 0.01$; Figure 7A). Gap junctions are made of connexins, with Cx43 being the most predominant gap junction protein in astrocytes (Giaume and McCarthy, 1996). Using quantitative real-time PCR, we found that Cx43 mRNA expression was 44% higher in *GFAP*$^{-/-}$*Vim*$^{-/-}$ in than WT astrocytes ($P < 0.05$; Figure 7B), further linking astrocyte IFs and AGJC.

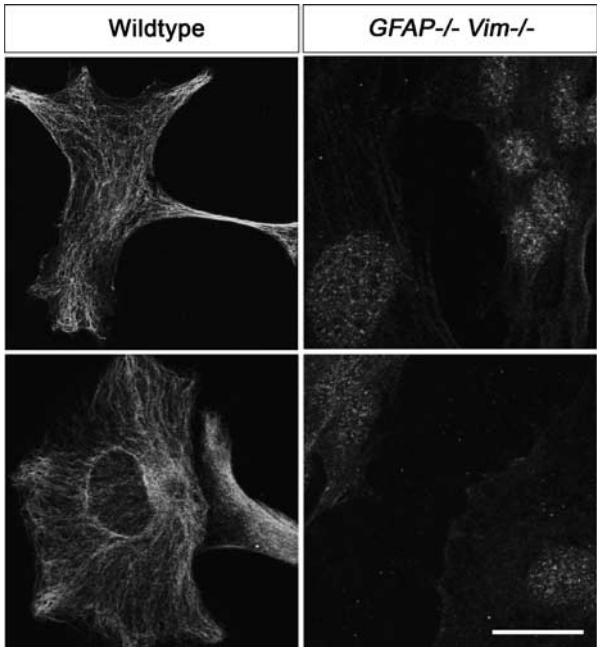

Figure 4 ET_BR immunoreactivity had a filamentous appearance in the cytoplasm of cultured WT astrocytes but was absent in the cytoplasm of *GFAP*$^{-/-}$*Vim*$^{-/-}$ astrocytes, where it was often confined to the cell nuclei. Green, ET_BR. Scale bar = 50 μm.

Reduction in Glutamate Transport in *GFAP*$^{-/-}$*Vim*$^{-/-}$ Mice

The ability of astrocytes to remove glutamate released by neurons was proposed to reduce infarct size by limiting the excitotoxic cell death (reviewed in Nedergaard and Dirnagl, 2005). To determine if glutamate transport is altered in *GFAP*$^{-/-}$*Vim*$^{-/-}$ mice, we examined total glutamate uptake and glutamate uptake mediated by GLT-1, the primary glutamate transporter in astrocytes, in freshly dissected hemicortices of *GFAP*$^{-/-}$*Vim*$^{-/-}$ and WT mice. Mean total glutamate uptake in *GFAP*$^{-/-}$*Vim*$^{-/-}$ mice was 44% lower than in WT controls (1.99 ± 0.79 vs $3.53 \pm$

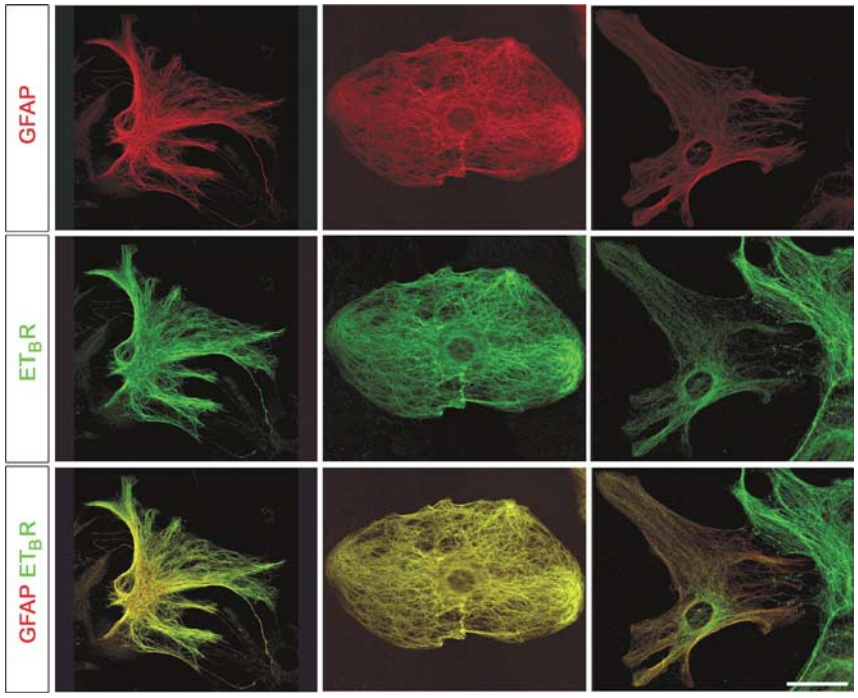

Figure 5 ET_BR and bundles of IFs colocalize in cultured WT astrocytes. Laser-scanning confocal microscopy revealed a filamentous appearance of ET_BR immunostaining, which colocalized with GFAP-positive bundles of IFs. Red, GFAP; green, ET_BR. Scale bar = 20 μm.

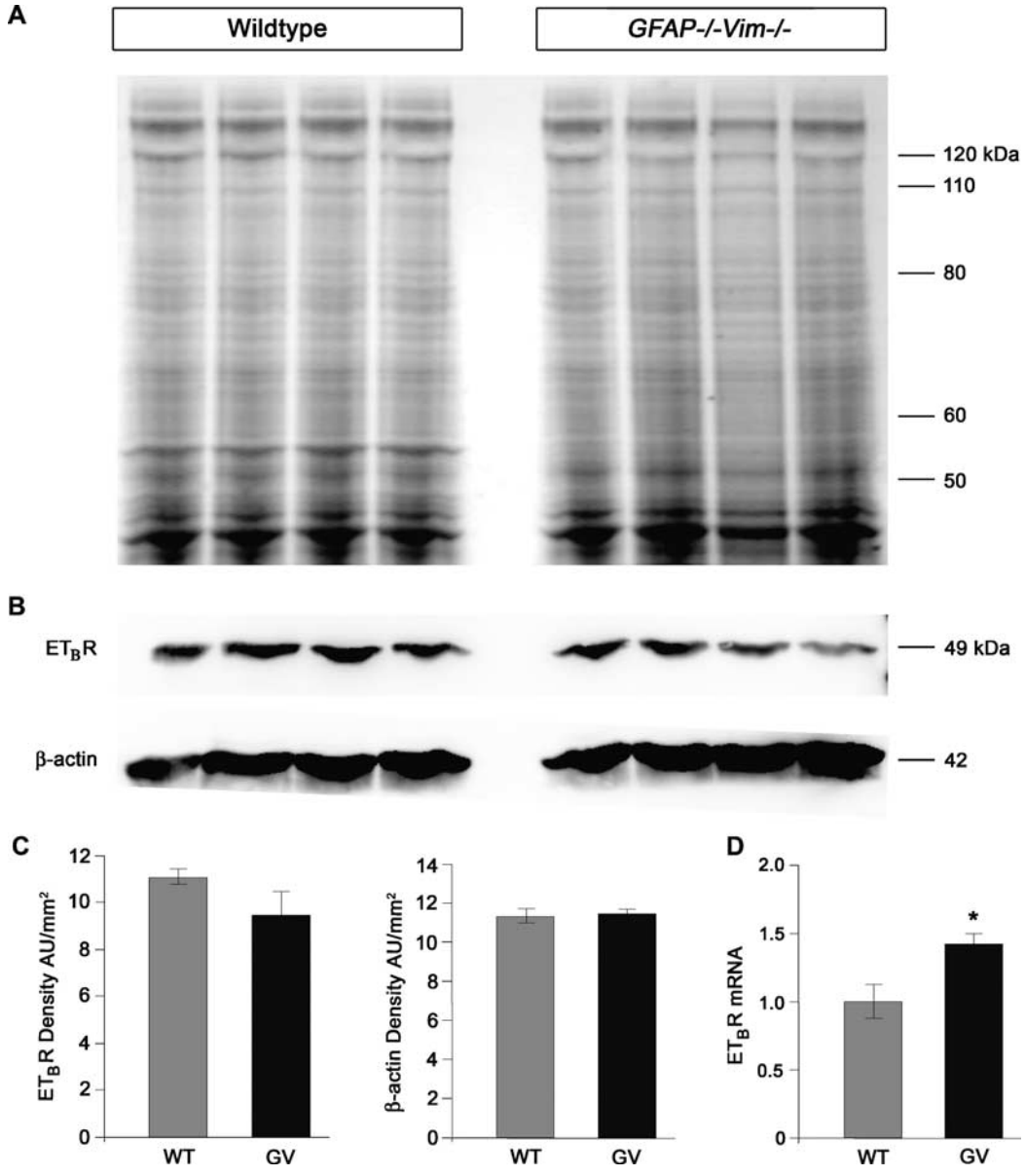

Figure 6 ET_BR protein levels are comparable in WT and *GFAP*$^{-/-}$*Vim*$^{-/-}$ (GV) cultured astrocytes. (**A**) Coomassie blue staining confirmed equal loading of protein. (**B**) Western blot analysis showed comparable levels of ET_BR protein in WT and *GFAP*$^{-/-}$*Vim*$^{-/-}$ astrocytes. β-Actin was used as a control. (**C**) Quantification of ET_BR protein levels from (**B**). (**D**) Quantitative real-time PCR showed higher levels of ET_BR mRNA in *GFAP*$^{-/-}$*Vim*$^{-/-}$ than in WT astrocytes ($^*P < 0.05$). Values are mean $\pm$ s.e.m. AU, arbitrary units.

0.17 nmol/mg per min; $P < 0.05$). Similarly, GLT-1-dependent transport was 50% lower than in WT mice (1.38 ± 0.78 vs 2.85 ± 0.29 nmol/mg per min, $P < 0.05$; Figure 8A). Western blot analysis showed comparable amounts of GLT-1 in WT and *GFAP*$^{-/-}$*Vim*$^{-/-}$ cerebral cortex (22 ± 3 vs 20 ± 4 U; Figures 8B and 8C) and immunohistochemical analyses of the ischemic penumbra showed less prominent GLT-1 immunostaining in astrocytes of *GFAP*$^{-/-}$*Vim*$^{-/-}$ compared with WT mice (Figure 8D). Thus, astrocytes of *GFAP*$^{-/-}$*Vim*$^{-/-}$ mice are less capable of removing glutamate from the ischemic brain tissue.

Plasminogen Activator Inhibitor-1 is Downregulated in *GFAP*$^{-/-}$*Vim*$^{-/-}$ Astrocytes

To address further, at a molecular level, the effect of attenuated reactive gliosis, we performed microarray analysis with the Atlas cDNA Expression Arrays (Clontech Laboratories). The expression of 1,200 genes was analyzed in primary astrocyte cultures derived from WT and *GFAP*$^{-/-}$*Vim*$^{-/-}$ mice and maintained in the presence of 10% serum. Only a single gene, *PAI-1*, an inhibitor of tissue plasminogen activator (tPA), fulfilled the criteria of a threefold or higher downregulation in *GFAP*$^{-/-}$*Vim*$^{-/-}$ than

in WT astrocytes (the ratio was 0.3 for *GFAP*$^{-/-}$ *Vim*$^{-/-}$/WT astrocyte cultures). Next, we performed quantitative real-time PCR analysis of PAI-1 mRNA in primary *GFAP*$^{-/-}$*Vim*$^{-/-}$ and WT astrocytes maintained in the presence of either 1 or 10% serum, the latter mimicking some aspects of reactive gliosis. Compared with WT, *GFAP*$^{-/-}$*Vim*$^{-/-}$ astrocytes showed a 69% reduction in PAI-1 mRNA in the presence of 1% serum ($P<0.05$), and an 86% reduction in 10% serum ($P<0.01$; Figure 9).

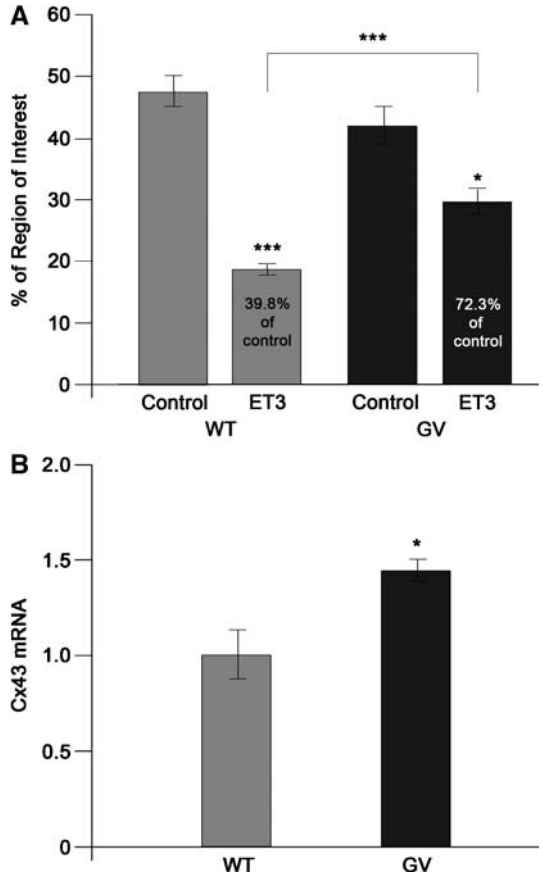

Figure 7 (**A**) Endothelin-3 (ET3)-induced blockage of gap junction is attenuated in *GFAP*$^{-/-}$*Vim*$^{-/-}$ (GV) astrocytes (*$P<0.05$ and ***$P<0.001$). (**B**) Quantitative real-time PCR shows higher levels of connexin 43 (Cx43) mRNA in *GFAP*$^{-/-}$*Vim*$^{-/-}$ than in WT astrocytes (*$P<0.05$). Values are mean $\pm$ s.e.m.

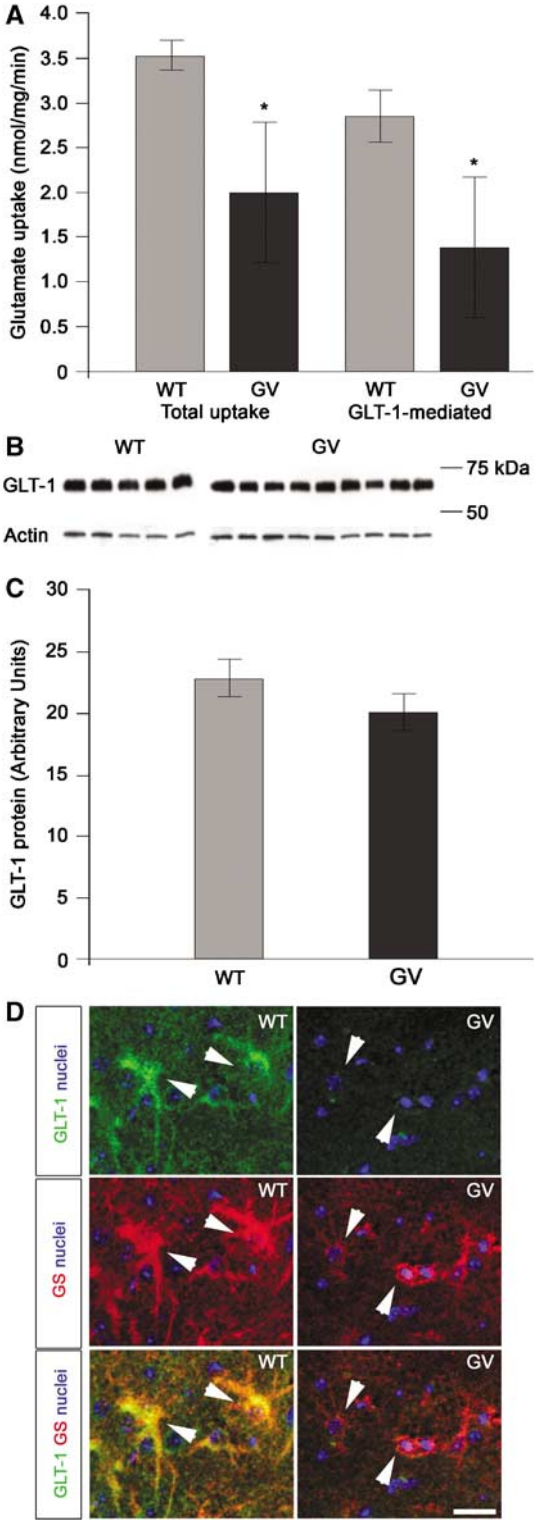

Figure 8 Total and GLT-1-mediated glutamate uptake is decreased in the cortex of *GFAP*$^{-/-}$*Vim*$^{-/-}$ (GV) mice. (**A**) Total and GLT-1-mediated glutamate uptake was lower in *GFAP*$^{-/-}$ *Vim*$^{-/-}$ than in WT mice (*$P<0.05$). (**B**) Western blot analysis showed comparable levels of GLT-1 protein in WT and *GFAP*$^{-/-}$*Vim*$^{-/-}$ astrocytes. Actin was used as a control. (**C**) Quantification of GLT-1 protein levels from (**B**). Values are mean $\pm$ s.e.m. (**D**) Glutamine synthase (GS)-positive astrocytes adjacent to the ischemic lesion in WT mice show distinct GLT-1 immunoreactivity, whereas in GV mice, GLT-1 immunoreactivity is less prominent. Arrowheads, astrocytes. Green, GLT-1; red, GS; nuclei visualized by ToPro-3. Scale bar = 25 μm.

Discussion

In the absence of a suitable experimental model, direct proof that astrocytes have a protective effect

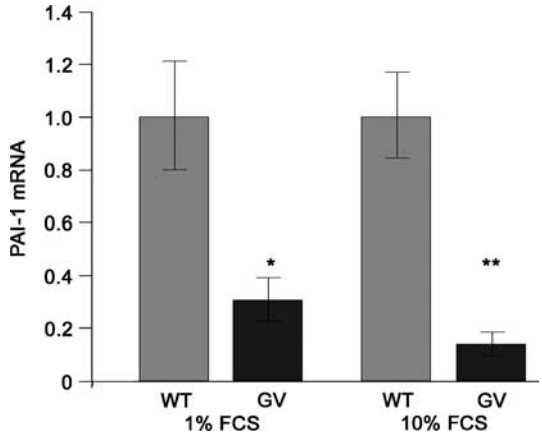

Figure 9 Plasminogen activator inhibitor-1 mRNA levels are lower in *GFAP*$^{-/-}$*Vim*$^{-/-}$ (GV) than in WT astrocytes cultured in the presence of 1 or 10% fetal calf serum (**$P < 0.01$ and *$P < 0.05$). Values are mean ± s.e.m.

in the ischemic brain has largely been lacking. Attempts to generate mammalian models in which astrocytes would be globally or regionally eliminated resulted in phenotypes too severe or complex for studying the role of astrocytes in the pathogenesis of CNS diseases. In mice expressing herpes simplex virus thymidine kinase from the GFAP promoter, ablation of dividing astroglial cells by treatment with ganciclovir during early postnatal development led to severe developmental abnormalities (Delaney *et al*, 1996). The same approach was applied in adult mice to selectively eliminate the subpopulation of dividing reactive astrocytes after neurotrauma and resulted in a massive invasion of leukocytes in response to dying astrocytes, increased neurodegeneration, and failed blood–brain barrier (BBB) repair (Bush *et al*, 1999), implying neuroprotective activities of astrocytes in the lesioned area (Faulkner *et al*, 2004).

Upregulation of IFs is a hallmark of reactive gliosis after trauma or stroke and is a key step in astrocyte activation (Pekny *et al*, 1999*b*). To address the role of reactive astrocytes in stroke, we subjected *GFAP*$^{-/-}$, *Vim*$^{-/-}$, and *GFAP*$^{-/-}$*Vim*$^{-/-}$ mice, which lack one or both of the key components of IFs in reactive astrocytes, to proximal or distal MCA transection. In three independent experiments, *GFAP*$^{-/-}$*Vim*$^{-/-}$ mice had 2- to 3.5-fold larger infarct volumes after 7 days of ischemia than WT controls. The infarct volumes in *GFAP*$^{-/-}$ or *Vim*$^{-/-}$ mice were not significantly different from those in WT mice. The increased infarct volumes in *GFAP*$^{-/-}$*Vim*$^{-/-}$ mice were linked to an altered distribution of ET_BR, less efficient ET_BR-mediated inhibition of AGJC, reduced ability to take up glutamate, and lower levels of tPA inhibitor PAI-1 in IF-free *GFAP*$^{-/-}$*Vim*$^{-/-}$ astrocytes. These results provide evidence that reactive astrocytes have a protective role in brain ischemia.

In *GFAP*$^{-/-}$ mice, reactive astrocytes contain reduced amounts of IFs, which are composed of vimentin and nestin (Eliasson *et al*, 1999; Pekny *et al*, 1998*a*). Reactive astrocytes in *Vim*$^{-/-}$ mice also contain reduced amounts of IFs, and the IF bundles are abnormally compact, reflecting reduced space between individual filaments (Eliasson *et al*, 1999). Despite these abnormalities, reactive astrocytes in these single-mutant mice were not compromised with regard to their function in stroke. However, the complete absence of IFs in reactive astrocytes in *GFAP*$^{-/-}$*Vim*$^{-/-}$ mice profoundly affected infarct volume. These results are consistent with the findings that healing after brain or spinal cord trauma was prolonged and synaptic loss was increased in *GFAP*$^{-/-}$*Vim*$^{-/-}$ mice, which have a complete deficiency of IFs in reactive astrocytes, but there was normal healing in *GFAP*$^{-/-}$ or *Vim*$^{-/-}$ mice, which have only a partial deficiency (Menet *et al*, 2003; Pekny *et al*, 1999*b*; Wilhelmsson *et al*, 2004). However, we cannot exclude the possibility that partial IF deficiency had a subtle effect that escaped detection. In another study, *GFAP*$^{-/-}$ mice and WT controls had similar infarct volumes after 2 days of permanent MCA occlusion; however, when MCA occlusion was combined with transient occlusion of the carotid artery, the *GFAP*$^{-/-}$ mice had larger infarcts than the controls (Nawashiro *et al*, 2000).

Vimentin is also expressed in other cell types in the CNS, particularly endothelial cells, oligodendroglia, and microglia. Endothelial cells in *Vim*$^{-/-}$ mice are devoid of IFs because the other IF protein expressed in these cells, nestin, cannot form filaments on its own (Eliasson *et al*, 1999; Pekny *et al*, 1999*b*). Thus, with regard to IF production in reactive astrocytes, the only difference between *Vim*$^{-/-}$ and *GFAP*$^{-/-}$*Vim*$^{-/-}$ mice is the partial or complete absence, respectively, of IFs. Since stroke volumes were not significantly different in *Vim*$^{-/-}$ mice and WT controls, the absence of IFs in endothelial cells and other cell types does not affect infarct size. *GFAP*$^{-/-}$*Vim*$^{-/-}$ and WT mice had comparable cerebrovascular architecture, as well as comparable mean blood pressure and heart rate before and during the focal brain ischemia. This implies that the increased infarct size after MCA transection in *GFAP*$^{-/-}$*Vim*$^{-/-}$ mice is a consequence of the absence of IFs in astrocytes.

How might the absence of IFs in reactive astrocytes explain the increased infarct size in *GFAP*$^{-/-}$*Vim*$^{-/-}$ mice? The lack of IFs may compromise several functions of astrocytes, namely AGJC, uptake and transport of molecules such as glutamate, glucose, and ascorbate, protection against tPA-mediated neurotoxicity, reconstruction of damaged BBB, migration into the injured area, and regulation of cell volume.

We saw a close colocalization between bundles of IFs and ET_BR immunoreactivity in cultured WT astrocytes and altered ET_BR immunoreactivity in *GFAP*$^{-/-}$*Vim*$^{-/-}$ astrocytes both *in vitro* and *in vivo*. These findings suggest that ET_BRs associate with IFs

and are freely distributed throughout the cell in IF-free astrocytes, which also exhibit less efficient ET_BR-mediated inhibition of AGJC. Astrocyte gap-junctional communication was proposed to promote secondary expansion of focal injury, since open astrocytic gap junctions can mediate the propagation of cell death signals or undesirable backflow of ATP from living to dying cells (Lin *et al*, 1998). Thus, less efficient ET_BR-mediated inhibition of AGJC in *GFAP*$^{-/-}$*Vim*$^{-/-}$ mice may have contributed to larger infarct volume in these mice.

Astrocytes play a major role in the transport and metabolism of a range of molecules, in particular those utilized in nutrition, cell–cell signaling, and neurotransmission. A failure to carry out these functions may constitute a major pathogenic component in stroke and other CNS pathologies (reviewed in Kraig *et al*, 1995). In primary cultures of reactive astrocytes from WT, *GFAP*$^{-/-}$, *Vim*$^{-/-}$, and *GFAP*$^{-/-}$*Vim*$^{-/-}$ mice, we found no differences in their ability to transport glucose and ascorbate (Pekny *et al*, 1999*a*). Previously, we showed that despite comparable availability of GS (Wilhelmsson *et al*, 2004), glutamine levels in reactive astrocytes from both *GFAP*$^{-/-}$ and *GFAP*$^{-/-}$*Vim*$^{-/-}$ mice were increased by 70 to 100% (Pekny *et al*, 1999*a*). Our present data show that glutamate transport is reduced in brain cortices of *GFAP*$^{-/-}$*Vim*$^{-/-}$ mice. It is tempting to speculate that the reduced ability of the *GFAP*$^{-/-}$*Vim*$^{-/-}$ mice to remove glutamate from the ischemic brain tissue, possibly due to deficient intracellular trafficking of GLT-1, is the consequence of intracellular glutamine accumulation. It was shown recently that GLT-1 immunoreactivity in astrocytes colocalized with bundles of IFs (Shobha *et al*, 2007) and GLT-1 trafficking and cluster formation within astrocyte processes were proposed to be dependent on the cytoskeleton (Zhou and Sutherland, 2004). Notably, *GLT-1*$^{-/-}$ mice show more extensive ischemia-induced damage (Mitani and Tanaka, 2003), and when *GLT-1*$^{+/-}$ mice are crossed to superoxide dismutase-1 (G93A) mice, a model of amyotrophic lateral sclerosis, they have more prominent loss of motor neurons and muscle strength than SOD-1 (G93A) mice alone (Pardo *et al*, 2006). These findings indicate that glutamate transporter dysfunction influences astrocyte–neuron interactions after injury.

Among 1,200 genes whose expression was compared between WT and *GFAP*$^{-/-}$*Vim*$^{-/-}$ astrocytes, *PAI-1* was the only gene that showed at least threefold downregulation in the mutants. Quantitative real-time PCR confirmed the downregulation of PAI-1 mRNA in *GFAP*$^{-/-}$*Vim*$^{-/-}$ astrocytes. Plasminogen activator inhibitor-1 inhibits tPA, which has a neurotoxic effect in the ischemic penumbra, probably mediated through the activation of both microglia and *N*-methyl D-aspartate receptors (Sheehan and Tsirka, 2005). Mice deficient in tPA have smaller infarcts than WT controls in a transient focal ischemia model, and administration of tPA to both tPA-deficient and WT mice increases infarct volume (Tsirka *et al*, 1995). Similarly, mice overexpressing PAI-1 have smaller infarcts than WT controls after focal brain ischemia (Nagai *et al*, 2005). Thus, reduced levels of PAI-1 mRNA could enhance the neurotoxic effects of tPA in the ischemic penumbra of *GFAP*$^{-/-}$*Vim*$^{-/-}$ mice.

Reactive astrocytes play a key role in the reconstruction of damaged BBB after both trauma and stroke. In a previous study with the *in vitro* BBB model, we demonstrated that IF-deficient astrocytes were either unable to induce BBB properties in endothelial cells or did so less efficiently (Pekny *et al*, 1998*b*). Thus, less efficient reconstruction of the BBB in the penumbra may contribute to the increased infarct volume in *GFAP*$^{-/-}$*Vim*$^{-/-}$ mice.

In response to CNS injury, astroglial cells migrate over considerable distances to the injured region, where they join the local pool of reactive astrocytes (Johansson *et al*, 1999). We have shown that partial or complete deficiency of IFs in reactive astrocytes *in vitro* reduces their ability to migrate (Lepekhin *et al*, 2001). However, since the overall number of astrocytes and microglia around the infarct area did not differ in *GFAP*$^{-/-}$*Vim*$^{-/-}$ and WT mice, reduced migration does not seem to contribute to the increased infarct volume.

The ability of astrocytes to regulate their volume by releasing osmotically active molecules, such as taurine, is considered to be a mechanism for counteracting cytotoxic brain edema in stroke (Kimelberg, 1991). When subjected to hypotonic stress, *GFAP*$^{-/-}$*Vim*$^{-/-}$ reactive astrocytes *in vitro* release 25 to 46% less taurine than WT controls, indicating a reduced capacity to counteract cell swelling (Ding *et al*, 1998) that could have contributed to the increased infarct volumes in *GFAP*$^{-/-}$*Vim*$^{-/-}$ mice. Consistent with this possibility, we showed that mice with IF-free nonreactive astrocytes have more prolonged changes in extracellular space diffusion parameters than WT controls during cell swelling evoked by hypotonic stress or high $[K^+]$ (Anderova *et al*, 2001).

Previously, we showed that attenuation of reactive gliosis in *GFAP*$^{-/-}$*Vim*$^{-/-}$ mice increases synaptic loss at the initial stage after neurotrauma, but allows complete synaptic regeneration later on (Wilhelmsson *et al*, 2004). Thus, reactive gliosis seems to play a positive role soon after CNS injury, although it seems to pose an obstacle to regeneration at a later stage (reviewed in Pekny and Pekna, 2004). The results of a recent study using conditional ablation of Stat3 and Socs3 also point to a dual role of reactive astrocytes after spinal cord injury (Okada *et al*, 2006). Here we show a similar neuroprotective effect of reactive gliosis in brain ischemia. Genetic ablation of astrocyte IFs led to altered intracellular distribution of ET_BR immunoreactivity in reactive astrocytes, both in the dentate gyrus affected by neurodegeneration induced by entorhinal cortex lesion (Wilhelmsson *et al*, 2004) and in ischemic

tissue as shown here. Thus, less efficient ET_BR-mediated inhibition of AGJC in *GFAP*$^{-/-}$*Vim*$^{-/-}$ astrocytes might contribute to both increased synaptic loss in the acute stage after entorhinal cortex lesion and to larger infarct volume after focal brain ischemia in these mice.

In summary, our findings provide *in vivo* evidence that reactive astrocytes play a protective role in ischemic stroke.

Acknowledgements

We thank Dr Anders Hamberger, Dr John Eriksson, and Hanna-Mari Pallari for their input in this project and Dr Martin Rydmark for his advice on stereomeric evaluation of the infarct volume.

References

Anderova M, Kubinova S, Mazel T, Chvatal A, Eliasson C, Pekny M, Sykova E (2001) Effect of elevated K(+), hypotonic stress, and cortical spreading depression on astrocyte swelling in GFAP-deficient mice. *Glia* 35:189–203

Blomstrand F, Giaume C, Hansson E, Ronnback L (1999) Distinct pharmacological properties of ET-1 and ET-3 on astroglial gap junctions and Ca(2+) signaling. *Am J Physiol* 277:C616–27

Bush TG, Puvanachandra N, Horner CH, Polito A, Ostenfeld T, Svendsen CN, Mucke L, Johnson MH, Sofroniew MV (1999) Leukocyte infiltration, neuronal degeneration, and neurite outgrowth after ablation of scar-forming, reactive astrocytes in adult transgenic mice. *Neuron* 2:297–308

Delaney CL, Brenner M, Messing A (1996) Conditional ablation of cerebellar astrocytes in postnatal transgenic mice. *J Neurosci* 16:6908–18

Ding M, Eliasson C, Betsholtz C, Hamberger A, Pekny M (1998) Altered taurine release following hypotonic stress in astrocytes from mice deficient for GFAP and vimentin. *Brain Res Mol Brain Res* 62:77–81

Eddleston M, Mucke L (1993) Molecular profile of reactive astrocytes—implications for their role in neurologic disease. *Neuroscience* 54:15–36

Eliasson C, Sahlgren C, Berthold CH, Stakeberg J, Celis JE, Betsholtz C, Eriksson JE, Pekny M (1999) Intermediate filament protein partnership in astrocytes. *J Biol Chem* 274:23996–4006

Faulkner JR, Herrmann JE, Woo MJ, Tansey KE, Doan NB, Sofroniew MV (2004) Reactive astrocytes protect tissue and preserve function after spinal cord injury. *J Neurosci* 24:2143–55

Fotheringham AP, Davies CA, Davies I (2000) Oedema and glial cell involvement in the aged mouse brain after permanent focal ischaemia. *Neuropathol Appl Neurobiol* 26:412–23

Giaume C, McCarthy KD (1996) Control of gap-junctional communication in astrocytic networks. *Trends Neurosci* 19:319–25

Gomi H, Yokoyama T, Fujimoto K, Ikeda T, Katoh A, Itoh T, Itohara S (1995) Mice devoid of the glial fibrillary acidic protein develop normally and are susceptible to scrapie prions. *Neuron* 14:29–41

Johansson CB, Momma S, Clarke DL, Risling M, Lendahl U, Frisen J (1999) Identification of a neural stem cell in the adult mammalian central nervous system. *Cell* 96:25–34

Kimelberg HK (1991) *Swelling and volume control in brain astroglial cells*. New York: Springer

Kinouchi R, Takeda M, Yang L, Wilhelmsson U, Lundkvist A, Pekny M, Chen DF (2003) Robust neural integration from retinal transplants in mice deficient in GFAP and vimentin. *Nat Neurosci* 6:863–8

Koyama Y, Takemura M, Fujiki K, Ishikawa N, Shigenaga Y, Baba A (1999) BQ788, an endothelin ET(B) receptor antagonist, attenuates stab wound injury-induced reactive astrocytes in rat brain. *Glia* 26:268–71

Kraig R, Lascola C, Caggiano A (1995) Glial response to brain ischemia, In: *Neuroglia* (Kettenmann H, Ransom BR, eds), New York: Oxford University Press, 964–76

Lepekhin EA, Eliasson C, Berthold CH, Berezin V, Bock E, Pekny M (2001) Intermediate filaments regulate astrocyte motility. *J Neurochem* 79:617–25

Liedtke W, Edelmann W, Bieri PL, Chiu FC, Cowan NJ, Kucherlapati R, Raine CS (1996) GFAP is necessary for the integrity of CNS white matter architecture and long-term maintenance of myelination. *Neuron* 17: 607–15

Lin JH, Weigel H, Cotrina ML, Liu S, Bueno E, Hansen AJ, Hansen TW, Goldman S, Nedergaard M (1998) Gap-junction-mediated propagation and amplification of cell injury. *Nat Neurosci* 1:494–500

Maeda K, Hata R, Hossmann KA (1998) Differences in the cerebrovascular anatomy of C57black/6 and SV129 mice. *NeuroReport* 9:1317–9

McCall MA, Gregg RG, Behringer RR, Brenner M, Delaney CL, Galbreath EJ, Zhang CL, Pearce RA, Chiu SY, Messing A (1996) Targeted deletion in astrocyte intermediate filament (Gfap) alters neuronal physiology. *Proc Natl Acad Sci USA* 93:6361–6

Menet V, Prieto M, Privat A, Gimenez y Ribotta M (2003) Axonal plasticity and functional recovery after spinal cord injury in mice deficient in both glial fibrillary acidic protein and vimentin genes. *Proc Natl Acad Sci USA* 100:8999–9004

Mitani A, Tanaka K (2003) Functional changes of glial glutamate transporter GLT-1 during ischemia: an *in vivo* study in the hippocampal CA1 of normal mice and mutant mice lacking GLT-1. *J Neurosci* 23:7176–82

Nagai N, De Mol M, Lijnen HR, Carmeliet P, Collen D (1999) Role of plasminogen system components in focal cerebral ischemic infarction: a gene targeting and gene transfer study in mice. *Circulation* 99:2440–4

Nagai N, Suzuki Y, Van Hoef B, Lijnen HR, Collen D (2005) Effects of plasminogen activator inhibitor-1 on ischemic brain injury in permanent and thrombotic middle cerebral artery occlusion models in mice. *J Thromb Haemost* 3:1379–84

Nawashiro H, Brenner M, Fukui S, Shima K, Hallenbeck JM (2000) High susceptibility to cerebral ischemia in GFAP-null mice. *J Cereb Blood Flow Metab* 20:1040–4

Nedergaard M, Dirnagl U (2005) Role of glial cells in cerebral ischemia. *Glia* 50:281–6

Okada S, Nakamura M, Katoh H, Miyao T, Shimazaki T, Ishii K, Yamane J, Yoshimura A, Iwamoto Y, Toyama Y, Okano H (2006) Conditional ablation of Stat3 or Socs3 discloses a dual role for reactive astrocytes after spinal cord injury. *Nat Med* 12:829–34

Pardo AC, Wong V, Benson LM, Dykes M, Tanaka K, Rothstein JD, Maragakis NJ (2006) Loss of the astrocyte

glutamate transporter GLT1 modifies disease in SOD1 (G93A) mice. *Exp Neurol* 201:120–30

Pekny M, Eliasson C, Chien CL, Kindblom LG, Liem R, Hamberger A, Betsholtz C (1998*a*) GFAP-deficient astrocytes are capable of stellation *in vitro* when cocultured with neurons and exhibit a reduced amount of intermediate filaments and an increased cell saturation density. *Exp Cell Res* 239:332–43

Pekny M, Eliasson C, Siushansian R, Ding M, Dixon SJ, Pekna M, Wilson JX, Hamberger A (1999*a*) The impact of genetic removal of GFAP and/or vimentin on glutamine levels and transport of glucose and ascorbate in astrocytes. *Neurochem Res* 24:1357–62

Pekny M, Johansson CB, Eliasson C, Stakeberg J, Wallen A, Perlmann T, Lendahl U, Betsholtz C, Berthold CH, Frisen J (1999*b*) Abnormal reaction to central nervous system injury in mice lacking glial fibrillary acidic protein and vimentin. *J Cell Biol* 145: 503–14

Pekny M, Leveen P, Pekna M, Eliasson C, Berthold CH, Westermark B, Betsholtz C (1995) Mice lacking glial fibrillary acidic protein display astrocytes devoid of intermediate filaments but develop and reproduce normally. *EMBO J* 14:1590–8

Pekny M, Pekna M (2004) Astrocyte intermediate filaments in CNS pathologies and regeneration. *J Pathol* 204:428–37

Pekny M, Stanness KA, Eliasson C, Betsholtz C, Janigro D (1998*b*) Impaired induction of blood–brain barrier properties in aortic endothelial cells by astrocytes from GFAP-deficient mice. *Glia* 22:390–400

Ridet JL, Malhotra SK, Privat A, Gage FH (1997) Reactive astrocytes: cellular and molecular cues to biological function. *Trends Neurosci* 20:570–7

Rothstein JD, Martin L, Levey AI, Dykes-Hoberg M, Jin L, Wu D, Nash N, Kuncl RW (1994) Localization of neuronal and glial glutamate transporters. *Neuron* 13:713–25

Sheehan JJ, Tsirka SE (2005) Fibrin-modifying serine proteases thrombin, tPA, and plasmin in ischemic stroke: a review. *Glia* 50:340–50

Shobha K, Vijayalakshmi K, Alladi PA, Nalini A, Sathyaprabha TN, Raju TR (2007) Altered *in-vitro* and *in-vivo* expression of glial glutamate transporter-1 following exposure to cerebrospinal fluid of amyotrophic lateral sclerosis patients. *J Neurol Sci* 254:9–16

Stahlberg A, Hakansson J, Xian X, Semb H, Kubista M (2004) Properties of the reverse transcription reaction in mRNA quantification. *Clin Chem* 50:509–15

Tsirka SE, Gualandris A, Amaral DG, Strickland S (1995) Excitotoxin-induced neuronal degeneration and seizure are mediated by tissue plasminogen activator. *Nature* 377:340–4

Wilhelmsson U, Li L, Pekna M, Berthold CH, Blom S, Eliasson C, Renner O, Bushong E, Ellisman M, Morgan TE, Pekny M (2004) Absence of glial fibrillary acidic protein and vimentin prevents hypertrophy of astrocytic processes and improves post-traumatic regeneration. *J Neurosci* 24:5016–21

Zhou J, Sutherland ML (2004) Glutamate transporter cluster formation in astrocytic processes regulates glutamate uptake activity. *J Neurosci* 24:6301–6